Target Structure-Induced Suppression of the Ionization Cross Section for Low-Energy Antiproton-Molecular Hydrogen Collisions: Theoretical Confirmation

I. B. Abdurakhmanov, A. S. Kadyrov, D. V. Fursa, and I. Bray

ARC Centre for Antimatter-Matter Studies, Curtin University, GPO Box U1987, Perth 6845, Australia

(Received 27 June 2013; published 25 October 2013)

Theoretical confirmation of the experimentally observed phenomenon [Knudsen *et al.*, Phys. Rev. Lett. **105**, 213201 (2010)] of target structure-induced suppression of the ionization cross section for low-energy antiproton-molecular hydrogen collisions is given. To this end a novel time-dependent convergent close-coupling approach to the scattering problem that accounts for *all* possible orientations of the molecular target, has been developed. The approach is applied to study single ionization of molecular hydrogen on the wide energy range from 1 keV to 2 MeV with a particular emphasis on low energies. Results for the orientation-averaged total single ionization cross section are compared with available experimental data and good agreement is found at low (< 20 keV) and high (> 90 keV) energies. A minor discrepancy is found within a small energy gap near the maximum of the cross section.

DOI: 10.1103/PhysRevLett.111.173201 PACS numbers: 34.10.+x, 34.50.Gb

Interest in antiproton-impact ionization of atoms and molecules has been growing recently [1]. One of the reasons for this development is the relevance of these processes to radiotherapy and oncology (see, e.g., Ref. [2] and references therein). In addition, the precise knowledge of energy loss by antiprotons due to ionizing collisions is important to research within the ALPHA Collaboration at CERN on antihydrogen formation and trapping for testing the *CPT* invariance [3] and gravitational behavior of antimatter at rest [4–6]. This knowledge is crucial also for the upcoming Facility for Antiproton and Ion Research (FAIR) [7] at GSI, where hydrogen is expected to be one of the dominant residual-gas molecules.

Measurements of the cross section for single nondissociative ionization of molecular hydrogen have been performed on a wide energy range from 2.4 keV to 1.6 MeV [8–10]. In particular, Ref. [10] experimentally established that at very low energies the cross section is suppressed and falls proportional to the projectile velocity. This was in a sharp contrast to the behavior of corresponding atomic cross sections [11–13].

The antiproton-molecular hydrogen collision system is of great interest from a fundamental point of view as well. It is the simplest prototype of ion-molecule scattering due to the relative simplicity of the target and the absence of the electron capture channel. However, in contrast to antiproton collisions with hydrogen [14] or helium [15] atoms, collisions with molecular hydrogen represent a greater challenge to theory due to the existence of additional degrees of freedom. The lack of spherical symmetry, which stems from the multicenter nature of the target, represents an additional challenge for both structure and subsequent scattering calculations. Consequently, the orientation of the molecular axis with respect to the direction of the incident antiproton plays a pivotal role in the reaction dynamics.

A number of theoretical approaches to the problem have been developed [16–20]. The complexity of the many-body Coulomb problem requires the use of certain approximations. In all available studies the antiproton motion was treated semiclassically by means of straight-line trajectories. This approximation is widely used in ion-atom and ion-molecule collisions. Its validity was recently demonstrated for antiproton collisions with atomic hydrogen and helium using a fully quantum-mechanical approach [21,22]. The main differences between theoretical approaches to $\bar{p}$ collisions with H_2 come from approximations made in order to simplify the description of the molecular hydrogen target. The earliest approaches employed a spherical effective one-electron approximation with the use of model potentials [16,17,19]. The main criteria in these approaches was to reproduce a reasonable binding energy by tuning model parameters. Not surprisingly, the approaches that use spherical potentials for modeling H_2 as a one-electron target are not sensitive to different molecular orientations. Despite some success at high energies all the approaches with the effective one-electron description of the molecular target produce total cross sections for single ionization significantly larger than experiment at energies below 20 keV. Recently, following application to the H_2^+ molecular ion [23,24], studies with a more accurate description of H_2 have been developed where the contributions of both electrons and both nuclei of the molecular target were taken into account using the Born-Oppenheimer approximation [18–20]. The approach of Pindzola and co-workers [19,20] also allows for two-electron processes, such as the double ionization of H_2 and single ionization leaving the residual target H_2^+ in any of the possible bound states. However, even these sophisticated approaches do not agree with experiment at low energies.

Thus, the remarkable result experimentally established in Ref. [10] about the low-energy suppression of the cross

section is not only quite unlike the observed behavior of corresponding atomic cross sections but in a sharp contrast to the results from the sophisticated theoretical calculations as well. In their recent review of the state of the art of antiproton-impact ionization of atoms and molecules, the authors of Ref. [1] emphasize the fact that even the most advanced theoretical calculations of ionization of molecular hydrogen disagree with the low-energy measurements of Ref. [10] and that the current state of affairs is not particularly clear. Using a simple adiabatic picture of ionization it has been suggested [1,10] that the reason for the suppression of the molecular cross section is due to a mechanism where, as the projectile comes close to one of the target nuclei, the closest electron moves toward the other nucleus, where it can stay bound until the departure of the projectile. This hints that it is the molecular structure which causes the suppression. However, the aforementioned elaborate two-electron molecular calculations have not been able to confirm the target structure-induced suppression of ionization evidenced by the experimental data.

We aim to resolve this disagreement between theory and experiment by utilizing a newly developed time-dependent approach, which is based on the ideas of the convergent close-coupling (CCC) method [25,26]. A novel and important feature of the method is that it accounts for *all* possible molecular orientations in an *ab initio* fully analytic manner. In contrast to the previous implementation of the CCC method for antiproton-atom collisions based on the exact time-independent Schrödinger equation for the total scattering wave function [21,22], here we follow the commonly used semiclassical formalism [27] and solve the time-dependent Schrödinger equation for the electronic part of the total scattering wave function. This is due to the fact that for atomic collisions involving heavy particles like antiprotons, the fully quantum-mechanical [22,28] and semiclassical (see, e.g., Refs. [29,30]) approaches give practically the same results in the entire energy range of practical interest, while the former requires significantly larger computational resources.

We define the laboratory frame where the incoming antiproton with velocity $\boldsymbol{v}$ is along the Z axis with the origin at the center of the molecular axis $\boldsymbol{d}$. In this frame the relative motion of the antiproton is approximated with a straight-line trajectory $\boldsymbol{R}(t) = \boldsymbol{b} + \boldsymbol{v}t$, where the impact parameter $\boldsymbol{b}$ points along the x axis. We expand the total (electronic) scattering wave function in terms of pseudostates Φ_α according to $\Psi(t, \boldsymbol{r}_1, \boldsymbol{r}_2, \boldsymbol{b}, \boldsymbol{d}) = \sum_\alpha A_\alpha(t, \boldsymbol{b}, \boldsymbol{d}) \exp(-i\epsilon_\alpha t)\Phi_\alpha(\boldsymbol{r}_1, \boldsymbol{r}_2, \boldsymbol{d})$, where $\boldsymbol{r}_1$ and $\boldsymbol{r}_2$ are the position vectors of the electron 1 and 2, respectively, ϵ_α is the energy of the pseudostate Φ_α. The expansion coefficients $A_\alpha(t, \boldsymbol{b}, \boldsymbol{d})$ define the probability of transitions into electronic bound and continuum states. The pseudostates Φ_α describing the target are constructed via diagonalization of the H_2 Hamiltonian in a set of antisymmetrized two-electron configurations built from Laguerre one-electron orbitals. The calculations are performed for each target symmetry characterized by the projection of the total orbital angular momentum m, parity π, and spin s. For antiproton scattering from the ground state of H_2, only states with $s = 0$ are required.

With this representation of the total scattering wave function the semiclassical Schrödinger equation can be transformed into a set of coupled-channel differential equations for the time-dependent coefficients $A_\alpha(t, \boldsymbol{b}, \boldsymbol{d})$,

$$i\frac{dA_\alpha(t, \boldsymbol{b}, \boldsymbol{d})}{dt} = \sum_\beta A_\beta(t, \boldsymbol{b}, \boldsymbol{d})\langle\Phi_\alpha|V(t, \boldsymbol{r}_1, \boldsymbol{r}_2, \boldsymbol{b}, \boldsymbol{d})|\Phi_\beta\rangle \times \exp[i(\epsilon_\alpha - \epsilon_\beta)t]. \quad (1)$$

Equation (1) is solved with the initial conditions $A_\alpha(t_0 = -\infty, \boldsymbol{b}, \boldsymbol{d}) = \delta_{\alpha 0}$, as the target is initially in the ground state Φ_0. The time-dependent interaction of the target electrons and nuclei with the projectile in the laboratory-fixed frame is given by

$$V(t, \boldsymbol{r}_1, \boldsymbol{r}_2, \boldsymbol{b}, \boldsymbol{d}) = -1/|\boldsymbol{R}(t) - \boldsymbol{d}/2| - 1/|\boldsymbol{R}(t) + \boldsymbol{d}/2| + 1/|\boldsymbol{R}(t) - \boldsymbol{r}_1| + 1/|\boldsymbol{R}(t) - \boldsymbol{r}_2|.$$

In contrast to atomic targets, which are spherically symmetric, for collisions with molecular targets the set of coupled equations (1) has to be solved for a given orientation of the molecule specified by vector $\boldsymbol{d}$. In order to find orientationally averaged transition probabilities calculations have to be performed for a large number of molecular orientations, which is computationally expensive. For this reason, in all previous studies that account for the multicenter nature of the target, the calculations were limited to only three orthogonal molecular orientations [18–20].

We have developed an alternative approach. Briefly, we express the matrix elements and time-dependent coefficients in Eq. (1) in the form where their molecular orientation-dependent parts are factored out according to

$$A_\alpha(t, \boldsymbol{b}, \boldsymbol{d}) = \sum_{\lambda\mu} \mathcal{A}^\alpha_{\lambda\mu}(t, b, d) D^{\lambda*}_{\mu, m_\alpha}(\phi_d, \theta_d, 0), \quad (2)$$

$$\langle\Phi_\alpha|V(t, \boldsymbol{b}, \boldsymbol{d})|\Phi_\beta\rangle = \sum_{\lambda\mu} \mathcal{V}^{\alpha\beta}_{\lambda\mu}(t, b, d) D^{\lambda*}_{\mu, m_\alpha - m_\beta}(\phi_d, \theta_d, 0), \quad (3)$$

where $\mathcal{A}^\alpha_{\lambda\mu}(t, b, d)$ are the probability amplitudes independent of the molecular orientation and $D^{\lambda*}_{\mu, m_\alpha}(\phi_d, \theta_d, 0)$ is the Wigner rotation matrix [31]. The expansion indices are limited by the maximum allowed total orbital angular momentum.

We substitute the expansion (2) into Eq. (1) and integrate over all orientations of the molecular axis $\boldsymbol{d}$, using properties of the Wigner D functions. After some algebra, the following coupled differential equations for the molecular-orientation-independent part of the scattering amplitude $\mathcal{A}^\alpha_{\lambda\mu}(t, b, d)$ can be derived

$$i\frac{d\mathcal{A}^{\alpha}_{\lambda\mu}(t,b,d)}{dt} = \sum_{\beta}\exp[i(\epsilon_{\alpha}-\epsilon_{\beta})t]\sum_{LM}\mathcal{A}^{\beta}_{LM}(t,b,d) \times \sum_{sq}\frac{2\lambda+1}{2L+1}C^{LM}_{\lambda\mu sq}C^{Lm_{\beta}}_{\lambda m_{\alpha}sm_{\beta}-m_{\alpha}} \times \mathcal{V}^{\alpha\beta}_{sq}(t,b,d), \quad (4)$$

with $C^{LM}_{\lambda\mu sq}$ denoting the Clebsch-Gordan coefficients [31]. This set of equations is solved subject to the initial conditions $\mathcal{A}^{\alpha}_{\lambda\mu}(t_0=-\infty,b,d)=\delta_{\alpha 0}\delta_{\lambda 0}\delta_{\mu 0}$. This boundary condition now also implies that at infinite distances the antiproton does not feel the anisotropic nature of the molecular target.

The present target structure calculations (see below) are performed utilizing the Born-Oppenheimer approximation with the internuclei distance fixed at the ground-state equilibrium value of $d = 1.4$ a.u.. In this approximation the orientationally averaged cross section for single ionization of H_2 can be found from the amplitude defined in the expansion (2) with the use of the orthogonality properties of the Wigner D functions

$$\sigma = \sum_{\alpha\in[\epsilon_{\alpha}\geq 0]}\sum_{\lambda\mu}\frac{2\pi}{2\lambda+1}\int_0^{\infty}|\mathcal{A}^{\alpha}_{\lambda\mu}(t=+\infty,b,d)|^2 b\,db. \quad (5)$$

The cross section for a particular molecular orientation can be calculated by combining all $\mathcal{A}^{\alpha}_{\lambda\mu}(t,b,d)$ according to Eq. (2). The consistency of the results for orientation-dependent cross sections calculated from solving Eq. (4) with those that are obtained from direct solution of Eq. (1) has been checked. Further details of the approach including the definition of $\mathcal{V}^{\alpha\beta}_{\lambda\mu}(t,b,d)$ will be given elsewhere.

The calculations presented below have been performed with $Z \equiv vt$ from -100 to $+100$ a.u. at all energies. The accuracy of the final results for the orientationally averaged ionization cross section has been checked by performing calculations with several structure models that differ in the value of maximum orbital angular momentum $l_{\max}$ and a number of one-electron Laguerre functions N_l. Convergence to within 5%, across the entire energy range, has been achieved with the target model consisting of 674 states, where $l_{\max}=4$, $N_l = 20 - l$, and the Laguerre basis exponential falloff 2. In the present calculations we have included all H_2 target states with the maximum value of angular momentum projection $m_{\max}$ to be equal to $l_{\max}$. To improve the accuracy of calculations, the Laguerre $1s$ orbital was replaced with the H_2^+ $1s\sigma_g$ state, which is obtained via diagonalization of the H_2^+ Hamiltonian in the same Laguerre basis. The full set of antisymmetric two-electron configurations comprises two separate sets. In the frozen-core $(1s, nlm)$ configurations, one electron is limited to the $1s$ orbital of the H_2^+ ion, while the other occupies any of the Laguerre orbitals (nlm). The other set takes all possible $(n'l'm', nlm)$ configurations with principle quantum numbers of Laguerre orbitals n' and $n \leq 3$. The frozen-core configurations allow for a square-integrable representation of the target continuum and they allow for coupling to the ionization channels in the scattering calculations. The primary reason for inclusion of the $(n'l'm', nlm)$ configurations is to increase the accuracy in accounting for electron-electron correlations in the ground and low-lying excited states. With this basis, the ground-state energy was $-1.164\,97$ a.u., which compares well with the accurate value of -1.1745 [32]. We have also checked the consistency of the calculations obtained using the present code with the previous fully quantum-mechanical results for the helium target [22], by taking the internuclear separation to zero (i.e., considering He as the united atom limit of H_2).

In Fig. 1 we compare our results for the total cross section for antiproton impact single-ionization of H_2 with the experiment [8–10], the effective one-electron calculations of Refs. [16,17], and two-electron calculations of Refs. [18,20]. The model calculations with an atomic hydrogenlike description of molecular hydrogen can give reasonable agreement with experiment at energies above 200 keV. One can see that present calculations that accurately include contributions from all molecular orientations are in good agreement with all measured data except on a small energy region from 20 to 90 keV. A comparative study of effects arising from averaging over all orientations will be given elsewhere.

After single nondissociative ionization, the residual ions of H_2^+ can dissociate before they reach the detector, provided they are in the vibrational continuum states. We estimate the fraction of the H_2^+ ions in the vibrational continuum using the Franck-Condon factors for transitions

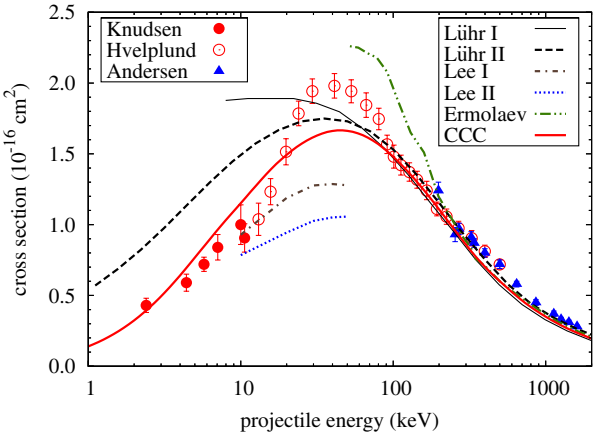

FIG. 1 (color online). The total cross section for single ionization of H_2 by antiprotons. Present CCC results are compared with the experimental data of Refs. [8–10], the one-electron calculations of [16], and two-electron calculations of Ref. [20] with (I) and without (II) allowance of excited H_2^+ states, and the calculations of Ref. [17,18] with an effective one-electron (I) and full two-electron (II) treatments of the target.

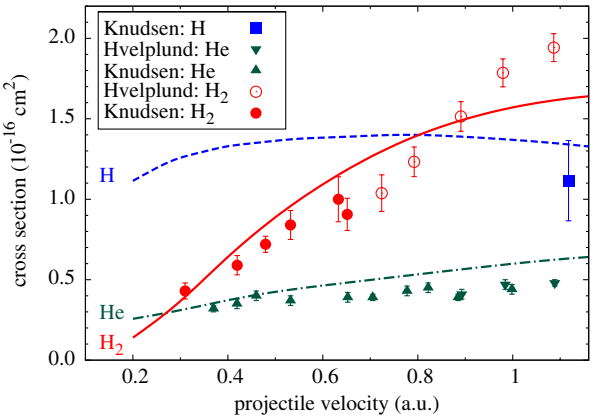

FIG. 2 (color online). The total cross section for single ionization of H_2, He, and H by low energy antiprotons. The curves are the CCC calculations. The experimental data for H are from Ref. [12], for He from Refs. [11,13], and for H_2 from Refs. [9,10].

from the ground vibrational level of H_2 into the all negative energy vibrational levels of H_2^+ [33]. We get that at most 1.7% of the residual H_2^+ ions may dissociate before reaching the detector. A similar estimate gives 0.5% for the D_2^+ ions used in the experiment. Thus, possible excitation of the vibrational continuum has little influence on the experimental result.

Though the CCC method gives the correct position of the maximum in the cross section, the experimental points exhibit a somewhat sharper maximum. Note that we did not include the vibrational degree of freedom. We assumed that the interaction time is much less than the period of vibrations. However, we have done a series of calculations with the internuclear distance varying from $0.85d$ to $1.15d$ and got linearly increasing cross sections. Thus the result presented in Fig. 1 at the equilibrium d is fully equivalent to the one that would follow from averaging for all possible internuclear distances. On the other hand, as mentioned above, for accurate results we had to solve our equations for Z ranging from -100 to $+100$ a.u., meaning that the interaction time is comparable with the period of vibrations in the ground state. Allowing for a time-dependent internuclear distance may improve the results.

In Fig. 2 we compare the present total cross section for single ionization of molecular hydrogen with those for single ionization of helium and atomic hydrogen at low energies as a function of the projectile velocity. The calculations accurately describe the behavioral change in the cross sections depending on the target structure as the velocity diminishes, exhibiting a strong suppression of

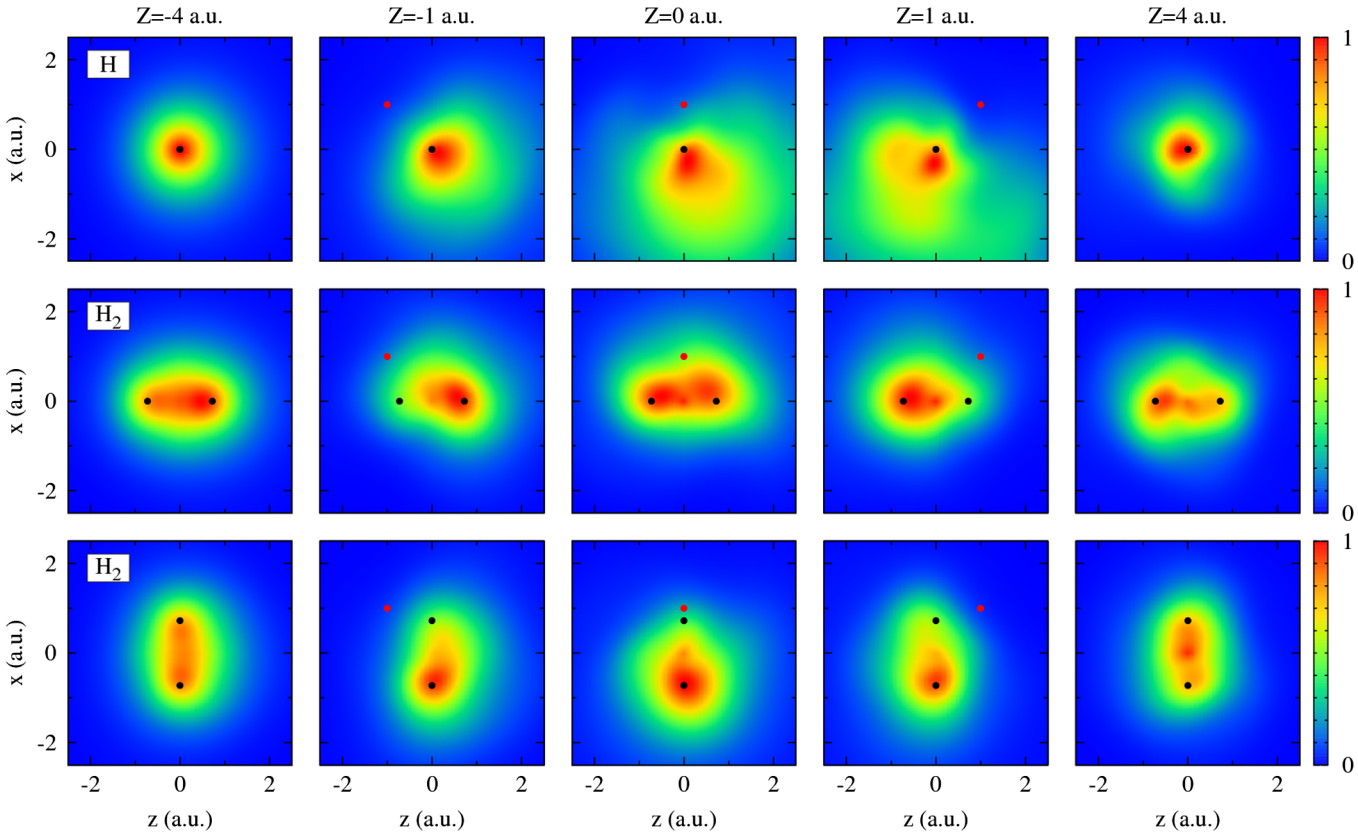

FIG. 3 (color online). The electron distribution dynamics in antiproton collisions with H and H_2 at 1 keV. The snapshots are taken at impact parameter $b = 1$ a.u. and several representative values of $Z = vt$. The corresponding projectile position is shown by gray (red online) dots. The protons are shown by black dots.

the cross section for the molecular target, in agreement with the data [9,10]. In order to see the differences in ionization mechanisms for the atomic and molecular targets we have calculated the distribution of the clouds for the active electron during the collision process. For this we first calculated $|\Psi(t, \boldsymbol{r}_1, \boldsymbol{r}_2, \boldsymbol{b}, \boldsymbol{d})|^2$, integrated over the coordinates of the passive electron $\boldsymbol{r}_2$. Then we integrate over the y component of the coordinates of the active electron $\boldsymbol{r}_1$ and plot the result in the scattering plane as a function of the x and z components of $\boldsymbol{r}_1$. For H it was only necessary to integrate $|\Psi|^2$ over y. The final probability distributions for each case have been normalized to the highest intensity. The electron distribution clouds are shown in Fig. 3 at the lowest velocity (0.2 a.u. corresponding to 1 keV) for antiproton collisions with H and H_2. The snapshots are taken at impact parameter $b = 1$ a.u. and several representative values of $Z = vt$ as indicated. The dynamics of the electron distribution for H is similar to the one seen in Ref. [34]. Differences are due to the fact that our cloud includes all states, both negative and positive energy ones, while Ref. [34] plotted only the part corresponding to ionization. The general feature of the cloud dynamics for H does not change much at low energies, leading to a relatively flat cross section as a function of energy commensurate with the Fermi-Teller limit [35]. The second and third rows in Fig. 3 depict the dynamics of the electron cloud for H_2 when the molecular target is oriented parallel and perpendicular to the direction of the projectile, respectively. They clearly show that whenever the antiproton approaches one of the protons, the electron takes a refuge at the other proton. This makes knocking out the electron more difficult, leading to suppression of the cross section. The effect tends to increase with the reduction of the projectile velocity as the electron has more time to escape. Therefore, the cross section for H_2 falls almost proportional to the velocity. We do not show the orientation when the target is perpendicular to the scattering plane. The situation here looks somewhat similar to the H one; however, as the projectile approaches, the cloud is distributed symmetrically with respect to the scattering plane. The results described above support the qualitative explanation given by Ref. [1].

There is a probability that some momentum will be transferred directly to one of the protons. This is most likely to happen when the molecular target is oriented perpendicular to the direction of the projectile; see Fig. 3. A simple estimate shows that, say for $b = 1$ a.u., an additional energy of about 1 eV can go to the vibrational states of H_2^+ through this mechanism. This means that states lying within 1 eV lower than the vibrational continuum may get lifted to the continuum. Then the Frank-Condon estimate for excitation of the vibrational continuum increases to 10% (8% for D_2^+). This effect is larger at smaller impact parameters. However, when calculating the cross section the transition probability at a given impact parameter is multiplied by the impact parameter [see Eq. (5)]. The latter reduces the contribution of the processes occurring at small impact parameters. Nevertheless, it would be interesting to investigate this effect quantitatively.

In conclusion, we have developed a novel time-dependent convergent close-coupling approach to the antiproton-impact ionization of H_2, which accounts for *all* possible orientations of the molecular target. The approach is valid at all energies, and significantly improves the agreement between theory and experiment, though some discrepancies remain. We have presented the first quantitative confirmation of the experimentally observed phenomenon of target structure-induced suppression of the ionization cross section for low-energy antiproton-molecular hydrogen collisions.

We thank Michael Charlton for helpful discussions. The work was supported by the Australian Research Council. We are grateful for access to the Australian National Computing Infrastructure Facility and its Western Australian node iVEC.

[1] T. Kirchner and H. Knudsen, J. Phys. B **44**, 122001 (2011).
[2] N. Bassler *et al.*, Radiother. Oncol. **86**, 14 (2008).
[3] C. Amole *et al.* (ALPHA Collaboration), Nature (London) **483**, 439 (2012).
[4] A. E. Charman *et al.* (ALPHA Collaboration), Nat. Commun. **4**, 1785 (2013).
[5] A. Kellerbauer *et al.*, Nucl. Instrum. Methods Phys. Res., Sect. B **266**, 351 (2008).
[6] P. Debu *et al.* (GBAR Collaboration), Hyperfine Interact. **212**, 51 (2012).
[7] Facility for Antiproton and Ion Research, www.fair-center.org.
[8] L. H. Andersen, P. Hvelplund, H. Knudsen, S. P. Moller, J. O. P. Pedersen, S. Tang-Petersen, E. Uggerhoj, K. Elsener, and E. Morenzoni, J. Phys. B **23**, L395 (1990).
[9] P. Hvelplund, H. Knudsen, U. Mikkelsen, E. Morenzoni, S. P. Moller, E. Uggerhoj, and T. Worm, J. Phys. B **27**, 925 (1994).
[10] H. Knudsen *et al.*, Phys. Rev. Lett. **105**, 213201 (2010).
[11] P. Hvelplund, H. Knudsen, U. Mikkelsen, E. Morenzoni, S. P. Moller, E. Uggerhoj, and T. Worm, J. Phys. B **27**, 925 (1994).
[12] H. Knudsen, U. Mikkelsen, K. Paludan, K. Kirsebom, and S. P. Møller, E. Uggerhøj, J. Slevin, M. Charlton, and E. Morenzoni, Phys. Rev. Lett. **74**, 4627 (1995).
[13] H. Knudsen *et al.*, Phys. Rev. Lett. **101**, 043201 (2008).
[14] D. R. Schultz, P. S. Krstic, C. O. Reinhold, and J. C. Wells, Phys. Rev. Lett. **76**, 2882 (1996).
[15] X. Guan and K. Bartschat, Phys. Rev. Lett. **103**, 213201 (2009).
[16] A. Ermolaev, Hyperfine Interact. **76**, 335 (1993).
[17] A. Lühr and A. Saenz, Phys. Rev. A **78**, 032708 (2008).
[18] A. Lühr and A. Saenz, Phys. Rev. A **81**, 010701 (2010).

[19] M. S. Pindzola, T.-G. Lee, and J. Colgan, J. Phys. B **43**, 235201 (2010).
[20] T. G. Lee, M. S. Pindzola, and J. Colgan, J. Phys. B **45**, 045203 (2012).
[21] I. B. Abdurakhmanov, A. S. Kadyrov, I. Bray, and A. T. Stelbovics, J. Phys. B **44**, 075204 (2011).
[22] I. B. Abdurakhmanov, A. S. Kadyrov, D. V. Fursa, I. Bray, and A. T. Stelbovics, Phys. Rev. A **84**, 062708 (2011).
[23] K. Sakimoto, Phys. Rev. A **71**, 062704 (2005).
[24] A. Lühr and A. Saenz, Phys. Rev. A **80**, 022705 (2009).
[25] I. Bray and A. T. Stelbovics, Phys. Rev. Lett. **70**, 746 (1993).
[26] I. Bray, D. V. Fursa, A. S. Kadyrov, A. T. Stelbovics, A. S. Kheifets, and A. M. Mukhamedzhanov, Phys. Rep. **520**, 135 (2012).
[27] B. H. Bransden and M. R. C. McDowell, *Charge Exchange and the Theory of Ion-Atom Collisions* (Clarendon, Oxford, 1992).
[28] I. B. Abdurakhmanov, I. Bray, D. V. Fursa, A. S. Kadyrov, and A. T. Stelbovics, Phys. Rev. A **86**, 034701 (2012).
[29] M. McGovern, D. Assafrão, J. R. Mohallem, C. T. Whelan, and H. R. J. Walters, Phys. Rev. A **81**, 032708 (2010).
[30] M. McGovern, C. T. Whelan, and H. R. J. Walters, Phys. Rev. A **82**, 032702 (2010).
[31] D. A. Varshalovich, A. N. Moskalev, and V. K. Khersonskii, *Quantum Theory of Angular Momentum* (World Scientific, Philadelphia, 1988), 1st ed.
[32] T. E. Sharp, At. Data Nucl. Data Tables **2**, 119 (1970).
[33] D. Wünderlich and U. Fantz, At. Data Nucl. Data Tables **97**, 152 (2011).
[34] B. Pons, Phys. Rev. Lett. **84**, 4569 (2000).
[35] E. Fermi and E. Teller, Phys. Rev. **72**, 399 (1947).